Lattice Model for Metal Ammonia Solutions

Kevin Leung and Félix S. Csajka
Department of Chemistry, University of California at Berkeley, Berkeley, California 94720
(Received 17 December 1996)

We study metal ammonia solutions using a generalized Kimball-Falicov model. The lattice model contains a fluid-fluid interaction term and an electron-fluid interaction with a hard core and an attractive tail. We derive the phase diagram using a strong-coupling mean field theory based on the slave boson approach to the Hubbard model. The attractive force favors the homogeneous phase and a regime where electrons localize in cavities devoid of fluid particles over phase separation. The Gaussian fluctuations suggest the existence of bicontinuous channels percolating through the system. Comparisons with experiments and computer simulations are presented. [S0031-9007(97)03061-5]

PACS numbers: 71.22.+i, 61.25.Mv, 71.10.Fd, 71.30.+h

Metal ammonia solutions exhibit a metal-insulator transition (MIT) and a variety of thermodynamic phases [1–3]. At low temperature, the system segregates into metal-rich and metal-poor phases [4]. At low metal concentration, the excess electrons are solvated in cavities surrounded by ammonia molecules [1,5]. They absorb light in the visible range, which gives the solution its characteristic blue color. These localized electrons contribute minimally to electrical conductivity. As the metal concentration increases, the electrical conductivity sharply increases by several orders of magnitude within a small concentration range [1–3]. Using computer simulations, Deng, Martyna, and Klein [6] have recently found that well-localized electron-containing cavities give way to bicontinuous percolating channels that support extended electronic states as the metal concentration increases. The crossover occurs at metal concentrations which are consistent with experimental data for the MIT. This strongly suggests that structural changes accompany the MIT.

Our model is a modified Kimball-Falicov model [7] in the strong-coupling limit. Excess electrons and ammonia molecules are represented as fermions and lattice gas particles ("blockers"), respectively. They interact through a hard-core repulsion and an attractive tail that mimicks the dipole- and screened charges-induced interactions. The metal counterions provide a neutralizing background [6], and electron-electron repulsion is neglected. In the strong-coupling form [8], the partition function is $\mathcal{Z} = \int \mathcal{D}'(\bar{\psi}\psi)\mathrm{Tr}_{\{n_i\}} e^{-S_o}$, where

$$S_o = -t \sum_{\langle ij\rangle\sigma} \int_\tau (1 - n_i)\bar{\psi}_{i\sigma\tau}\psi_{j\sigma\tau}(1 - n_j) - \sum_{ij\sigma}(1 - n_i)\int_\tau \bar{\psi}_{i\sigma\tau}\left[v_{ij}n_j + \delta_{ij}\left(\mu_e - \frac{\partial}{\partial\tau} - \lambda_i\right)\right]\psi_{i\sigma\tau}$$
$$- \sum_i(\mu_b - \xi_i)n_i - (1/2)\sum_{ij} n_i w_{ij} n_j \,. \tag{1}$$

$(\bar{\psi}_{i\sigma\tau}, \psi_{i\sigma\tau})$ are Grassmann (fermionic) fields for site i, spin σ, and Euclidean time index τ, $n_i = 0, 1$ describes the blocker occupancy of site i, and λ_i and ξ_i are generating fields. v_{ij} and $w_{ij} > 0$ are fermion-blocker and blocker-blocker attractive forces, respectively. μ_e and μ_b are the chemical potentials, and $\beta = \hbar = 1$. We apply the constraint that blockers and fermions cannot simultaneously occupy the same site. This on-site exclusion and the attractive interaction v_{ij} compete with each other. The model can be thought of as the quantum analog of a classical lattice model [9] that features short-ranged, competing forces and describes the lamella and bicontinuous microemulsion phases of oil-water-surfactant mixtures [10]. The physics of the two problems is very similar. v_{ij} herein plays the role of surfactant molecules, tying together the dissimilar fermion and blocker phases to form cavities and bicontinuous structures [6].

The exclusion constraint is difficult to implement in practice except in special cases [11]. In this work, we remove the constraint by introducing auxillary fermions at a modified chemical potential $(1 - \alpha)\mu_e$ on $n_i = 1$ sites. The action is augmented by

$$S_{\mathrm{aux}} = -\sum_{i\sigma} n_i \left\{ \int_\tau \bar{\psi}_{i\sigma\tau}\left[(1 - \alpha)\mu_e - \frac{\partial}{\partial\tau} - \lambda_i\right] \times \psi_{i\sigma\tau} - \Lambda_i \right\}, \tag{2}$$

where $\Lambda_i = \ln[1 + e^{\mu_e(1-\alpha)-\lambda_i}]$ and α is arbitrary. When $n_i = 1$, $(\bar{\psi}_{i\sigma\tau}, \psi_{i\sigma\tau})$ describe auxillary fermions that do not exhibit hopping, whose free energy contribution Λ_i per spin has been subtracted out in Eq. (2). $(S_o + S_{\mathrm{aux}})$ now has $2N$ unconstrained fermionic and N blocker degrees of freedom which can be decoupled using the Hubbard-Stratonovich transform [12,13]. We

introduce scalar fields $\{\phi_i, \sigma_i\}$ governed by the action

$$S' = \sum_{ij} \phi_i u_{ij}^{-1} \sigma_j + (1/2) \sum_{ijkl} \phi_i u_{ij}^{-1} w_{jk} u_{kl}^{-1} \phi_l . \quad (3)$$

At low fermion density, the diagonal term in $u_{ij} = -\alpha\mu_e\delta_{ij} + v_{ij}$ dominates and makes this matrix positive definite and invertible. Next we apply the transformations $\sigma_i \to \sigma_i + \sum_{j\sigma}\int_\tau u_{ij}\bar{\psi}_{j\sigma\tau}\psi_{j\sigma\tau}$ and $\phi_i \to \phi_i + \sum_j u_{ij} n_j$, whereupon any n_i coupled to Grassmann fields can be replaced by $-\sum_j u_{ij}^{-1}\phi_j$. The action becomes

$$S = S' - \sum_{i\sigma}\int_\tau \bar{\psi}_{i\sigma\tau}\left(\mu_e - \frac{\partial}{\partial\tau} - \phi_i - \lambda_i\right)\psi_{i\sigma\tau} - t\sum_{\langle ij\rangle\sigma}\int_\tau\left(1 + \sum_k u_{ik}^{-1}\phi_k\right)\bar{\psi}_{i\sigma\tau}\psi_{j\sigma\tau}\left(1 + \sum_l u_{jl}^{-1}\phi_l\right)$$
$$+ \sum_{ijkl\sigma}\int_\tau \phi_k u_{ki}^{-1}\bar{\psi}_{i\sigma\tau}\psi_{i\sigma\tau} v_{ij} u_{jl}^{-1}\phi_l - \sum_i(\mu_b - 2\Lambda_i - \sigma_i - \xi_i)n_i + \sum_{ijk}\phi_i u_{ij}^{-1} w_{jk} n_k . \quad (4)$$

The translation-invariant saddle point obtains by integrating over $(\bar{\psi}, \psi)$ and n_i, and minimizing with respect to $\phi_i \equiv \bar{\phi}$, $\sigma_i \equiv \bar{\sigma}$, and α. The Helmholtz free energy per site, $\bar{f}$, then becomes

$$\bar{f} = 2\int_k \ln(1-\rho_k) + \ln(1-\rho_b) - (\bar{\sigma} - w_o\rho_b/2)\rho_b ,$$
$$\bar{\sigma} = -2u_o\bar{\rho}_e + 4(1-\rho_b)\langle\epsilon\rangle + 4(u_o + \alpha\mu_e)\bar{\rho}_e\rho_b ,$$
$$\bar{\phi} = -u_o\rho_b, \quad \text{and} \quad \bar{\rho}_e = [1 + e^{-(1-\alpha)\mu_e}]^{-1}. \quad (5)$$

Here $\rho_k = \{1 + e^{-\bar{\Delta}_k - \mu_e + \bar{\phi} + (u_o + \alpha\mu_e)\rho_b^2}\}^{-1}$, $\bar{\rho}_e = \int_k \rho_k$ is the apparent fermion density, ρ_b is the blocker density, $\langle\epsilon\rangle$ denotes the average kinetic energy, $\bar{\Delta}_k$ equals $(1-\rho_b)^2$ times the energy of plane waves with wave vector k, $u_o = \sum_j u_{ij}$, and $w_o = \sum_j w_{ij}$. $\bar{f}$ is proportional to the pressure. The mean field theory has the following features: (a) For purely fermion-blocker exclusion interactions, it is exact in the $t \to 0$ limit. (b) The real single-spin fermion density is $\rho_e = -(1/2)\partial\bar{f}/\partial\mu_e = (1-\rho_b)\bar{\rho}_e$ [14]. Therefore $\rho_b + \rho_e \le 1$, and the exclusion constraint is satisfied on the average. (c) The hopping matrix element is renormalized by $\bar{t} \to (1-\rho_b)^2 t$. Qualitatively similar features are found in the slave boson approach to the Hubbard model [15,16]. A finite on-site interaction version of this method and a Gibbs-Bogoliubov variational derivation of Eq. (5) are given in Ref. [17]. The mean field theory is solved at constant pressure, temperature, and chemical composition $\chi_b = \rho_b/(\rho_b + 2\rho_e)$. The coexistence curves are found by graphically matching two solutions that have identical chemical potentials.

Gaussian fluctuations are computed by transforming the various fields to their Fourier space representation, integrating out $\{\bar{\psi}, \psi\}$ and $\{n_i\}$, expanding the resulting free energy to second order in $\delta\hat{\phi}_k$, $\delta\hat{\sigma}_k$, $\hat{\xi}_k$, $\hat{\lambda}_k$, and linear combinations thereof, and integrating out $\delta\hat{\phi}_k$ and $\delta\hat{\sigma}_k$:

$$-f^{(2)} = -(1/2)\int_k \ln(-\hat{u}_k^2 D_k) - \rho_b\bar{\rho}_e(1-\bar{\rho}_e)\int_k |\lambda_k|^2 - \int_k (1/2D_k)\mathbf{A}_k \cdot \begin{bmatrix} M_k^{\sigma\sigma} & -M_k^{\sigma\phi} \\ -M_k^{\sigma\phi} & M_k^{\sigma\sigma} \end{bmatrix} \cdot \mathbf{A}_{-k}$$
$$+ \int_{k_1,k_2}\left(\frac{\rho_{k_1} - \rho_{k_2}}{\bar{\Delta}_{k_1} - \bar{\Delta}_{k_2}}\right)\delta_{k-k_1+k_2}|\hat{\lambda}_k|^2 + (1/2)\int_k M_k^{\sigma\sigma}|\hat{\xi}_k - 2\bar{\rho}_e\hat{\lambda}_k|^2, \quad (6)$$

where $D_k = M_k^{\phi\phi}M_k^{\sigma\sigma} - |M_k^{\phi\sigma}|^2$, $\mathbf{A}_k$ is the two component vector $[M_k^{\phi\lambda}\hat{\lambda}_k + M_k^{\phi\xi}\hat{\xi}_k, M_k^{\sigma\sigma}(\hat{\xi}_k - 2\bar{\rho}_e\hat{\lambda}_k)]$, and $M_k^{\sigma\sigma}$ (for example) is $\partial^2 \ln\mathcal{Z}/\partial|\hat{\sigma}_k|^2 = \rho_b(1-\rho_b)$. The structure factors obtain by functionally differentiating $(-f^{(2)})$ with respect to $\hat{\lambda}_k$ and $\hat{\xi}_k$.

The localized fermions of the cavity regime cannot be described by the extended fermion formalism. Instead, we assume the system is a superlattice made up of identical rectangular cells of volume V_a. Fluctuations in cell size and shape are neglected. Each cell contains either fermions or blockers but not both. The fermion-containing cells are the cavities, and no fermion hopping between cells is permitted. The discrete fermion and blocker states within each cell are enumerated, and v_{ij} and w_{ij} between different cells are treated to mean field order. The fermion levels are further constrained so that their energies do not exceed the *mobility edge* estimated via Eq. (5) [17]. This constraint does not affect the phase diagrams significantly. The Gibbs free energy per molecule is optimized with respect to the discrete V_a, and compared to that of phase segregation and/or the extended fermion phase to determine the stable thermodynamic phase.

In the classical $t \to 0$ limit, $V_a = 1$ lattice site is optimal, and the localized and extended fermion theories are identical. When two-phase coexistence is stable, $V_a \to \infty$, and the localized and extended fermion phase free energies agree with each other. Hence the two theories agree in the high and low temperature limits.

We consider the various interaction terms step by step to illustrate the minimal requirements of a model that reproduces the thermodynamic phases and correlation functions. First we consider a purely excluded volume interaction ($v_{ij} = w_{ij} = 0$), Fig. 1(a). At high temperature, the thermal de Broglie wavelength is small, and fermions and blockers readily mix. At low temperature, fermions are highly degenerate, and phase segregation is energetically favored. The dotted line marks the onset of instability in the mean field solution. Along this line, D_k vanishes at $k = 0$ and the fluctuations diverge. The critical point of phase coexistence and the turning point of

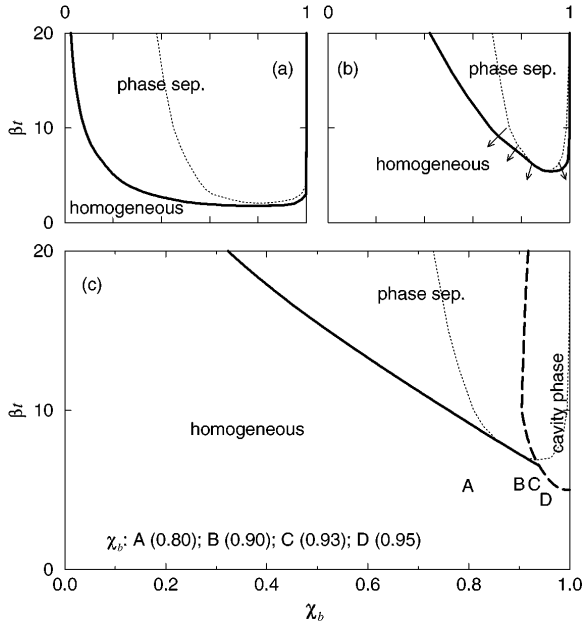

FIG. 1. Mean field phase diagrams. (a) $\beta P = 0.6$, excluded volume interaction only; (b) $\beta P = 0.6$, with attractive fermion-blocker tail; (c) $\beta P = 0.65$, with both fermion-blocker and blocker-blocker attraction. Dashed line: boundary of the cavity phase; dotted lines: onset of instability. In (b), the arrows indicate the emergence of modulate phases as ϵ increases.

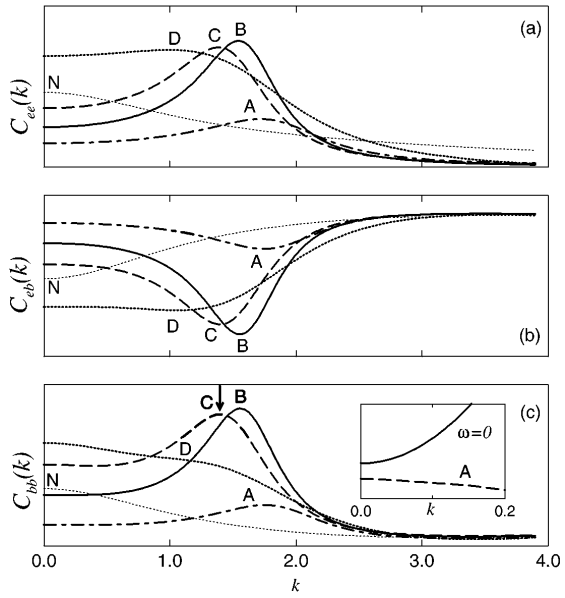

FIG. 2. Structure factors. (a) Electron-electron; (b) electron-blocker; (c) blocker-blocker. "N" (dotted line): sample structure factors for Fig. 1(a). "A"–"D" label structure factors at points indicated in Fig. 1(c). The cross correlations are negative. The y axes have been shifted and rescaled. Inset: small-k behavior of $\hat{C}_{bb}(k)$ at point A in Fig. 1(c) and $\chi_b = 0.8$ in Fig. 1(b), on an expanded scale. Arrow: peak position at 9% Li molar fraction ($\chi_b = 0.91$) computed in Ref. [6].

the instability line do not coincide due to the introduction of auxillary fermions. No cavity-dominated regime is found in the absence of attractive interactions, and the optimal cavity size is $V_a \to \infty$. The structure factors exhibit Ising-like behavior, peaking at $k = 0$ (Fig. 2).

Next we apply a square well potential $v_{ij} = \epsilon = 0.1$ for $i \neq j$, $|\mathbf{r}_i - \mathbf{r}_j|_{x,y,z} \leq 1$ [Fig. 1(b)]. The attractive interaction favors the homogeneous phase over phase separation. The low χ_b branch of the instability line marks the points where D_k first vanishes at *finite* k. $\epsilon > 0$ also stabilizes cavities: Fermions can reside in cavities devoid of blockers, lowering the kinetic energy while benefiting from the fermion-blocker attractive interaction at the cavity boundary. $\epsilon = 0.1$ is insufficient to induce a cavity-dominated regime. Further increasing ϵ results in the finite k-instabilities preempting the coexistence curve [Fig. 1(b)]. This is the signature of modulated phases, which also occur in lattice models for oil-water-surfactant mixtures [9,18] and Kimball-Falicov models with finite on-site fermion-blocker interactions [19].

Metal ammonia solutions phase separate at low temperatures; they do not form modulated phases. In Fig. 1(c), we further apply a square well potential between blockers, $w_{ij} = \omega = 0.002$ for $i \neq j$, $|\mathbf{r}_i - \mathbf{r}_j|_{x,y,z} \leq 2$, and increase ϵ to 0.16. w_{ij} stabilizes the two-phase region with respect to periodic phases at low temperature. A narrow strip dominated by cavities now appears at intermediate temperatures. These cavities are occupied by one localized fermion of each spin. At high temperature, extended states are more readily populated than localized states, while phase segregation occurs at low temperature. Since different theories are used for the extended and localized fermions, we do not equate their chemical potentials to establish phase coexistence.

Figure 2 plots the structure factors at points A–D in Fig. 1(c). $\hat{C}_{ee}(k)$, $\hat{C}_{bb}(k)$, and $\hat{C}_{eb}(k)$ all exhibit structures at $k_c = 1$ to 1.8. By comparison, the all-atom structure factor computed at $\chi_e = 1 - \chi_b = 0.09$ in Ref. [6] peaks at $(k\sigma_{\mathrm{NH}_3})_c = 1.4$ [Fig. 2(c)], where σ_{NH_3} is the ammonia Lennard-Jones diameter. This peak arises from the bicontinuity, and characterizes the mean separation between the percolating channels [6]. Our structure factors, derived by assuming that the fermions percolate through space, therefore strongly suggest that our model exhibits bicontinuity, with percolating channels 3–6 lattice sites apart. k_c decreases with decreasing χ_e and eventually vanishes for $\chi_e > 0$. The positions of "superstructure" peaks or shoulders observed in Li- and Na-NH_3 small-angle x-ray scattering [20] and small-angle neutron-scattering [21] experiments also shift towards $(k\sigma_{\mathrm{NH}_3})_c = 0$ as χ_e decreases. Our results and Ref. [6] suggest that these hitherto unexplained trends are due to the increasing separation of percolating channels. The electrical conductivity should be sensitive to such structural changes [23]. The $\hat{C}_{bb}(k)$'s for the system depicted in Fig. 1(c) and experimental structure factors [20] all contain $k = 0$ components. In our model, these features reflect $w_{ij} > 0$, and are absent for structure

factors computed at $\omega = 0$ [see inset of Fig. 2(c)], whose intermediate k behavior are otherwise similar [17].

The theoretical k_c [experimental Li-NH_3 $(k\sigma_{NH_3})_c$] values are 0.95 (1.3), 1.55 (2.1), and 1.70 (3.1) at $\chi_e = 0.044$, 0.10, and 0.16, respectively. Quantative comparison for $\chi_e < 0.04$ is hampered by the small shoulders predicted by the theory. While experiments, theory, and simulations are in reasonable agreement for $\chi_e \leq 0.1$, the lattice model does not model the fluid accurately at small length scales. $(k\sigma_{NH_3})_c$ is sensitive to the identity of the cation [20]. The functional form of v_{ij} can be varied to model this dependency.

To analyze the peak position, which is relatively temperature independent, we consider low temperature and small ρ_e. First let $\omega = 0$, whereupon $\hat{C}_{bb}(k)$ (modulo a constant) is entirely due to the fermions, and its small k behavior determines k_c. Furthermore, $M_k^{\phi\xi} = 0$ and $M_k^{\phi\sigma} = \hat{u}_k^{-1}$. From Eq. (6), we have

$$\hat{C}_{bb}(k) \propto \frac{1}{(\mathcal{M}_k)^{-1} - 1} \sim \frac{1}{M_o + M_2 k^2 + O(k^4)}; \quad (7)$$

$\mathcal{M}_k$ is $\rho_b(1-\rho_b)M_k^{\phi\phi}\hat{u}_k^2$, $M_o = \mathcal{M}_o^{-1} - 1 > 0$ due to mechanical stability, $M_2 = -(1/2\mathcal{M}_o^2)\partial^2\mathcal{M}_k/\partial k^2|_{k=0} \propto (k_F^{-2} - c\epsilon)$, $k_F = (6\pi^2\rho_e)^{1/3}$, and the positive scalar c is predominantly ρ_e independent. At large k_F and ϵ, $M_2 < 0$. From Eq. (7), this means that $k_c > 0$, and $\hat{C}_{bb}(k)$ [Fig. 2(c), inset] exhibits the characteristic form of microemulsionlike structure factors [22]. In microemulsions, the surface tension is small, which favors segregation of the pure species on mesoscopic/microscopic length scales and leads to bicontinuity [9]. In our model, as ρ_e decreases, k_F decreases, M_2 eventually changes sign, and k_c vanishes. This analysis shows that the superstructure in $\hat{C}_{bb}(k)$ arises from the competition between the fermion kinetic energy (the k_F^{-2} term) and the fermion-blocker attraction, i.e., it has the same origin as the cavity states. Furthermore, it is a purely quantal effect, absent for $t \to 0$.

At $\omega = 0.16$, the phases of metal ammonia solutions are reproduced. At this ω, M_2 is always positive, and $\hat{C}_{bb}(k)$ has a $k = 0$ peak over the entire χ_b range (Fig. 2), in agreement with experiments. The $\hat{C}_{bb}(k)$'s are therefore not microemulsionlike for small k. However, at length scales of 3–6 lattice sites, the superstructures persist, and the physics that governs microemulsions applies.

Our metal-insulator transition (the boundary between the cavity phase and the extended fermion phase) occurs at $\chi_e < 0.07$, depending on the temperature. MIT's occur at $\chi_e \sim 0.04$ in metal ammonia solutions. The cavity phase is more prominent at larger v_{ij} and lower pressure. At $\beta P = 0.4$ and $\epsilon = 0.175$, the MIT shifts to $\chi_e = 0.14$, comparable to the MIT ($\chi_e \sim 0.15$) in metal methylamine solutions [2], which have similar properties.

Despite the simplicity of our model, the present work predicts phase diagrams, superstructures, and metal insulator transitions that qualitatively agree with those found in metal ammonia solutions.

One of us (F. S. C.) acknowledges financial support from David Chandler. K. L. is indebted to Professor K. B. Whaley. We also thank Hyung-June Woo, Carlo Carraro, and Richard Stratt for useful suggestions, and David Chandler for suggesting a lattice model treatment.

[1] *Colloque Weyl VI, International Conference on Metals in Solution* [J. Phys. Chem. **88**, 3699 (1984)].
[2] *Colloque Weyl VII, International Conference on Metals in Solution* [J. Phys. IV **1** (1991)].
[3] Z. Phys. Chem. **184**, 1–172 (1994).
[4] P. Chieux *et al.*, J. Phys. IV **1**, 3 (1991), and references therein.
[5] Z.-H. Deng, G. J. Martyna, and M. L. Klein, Phys. Rev. Lett. **68**, 2496 (1992).
[6] Z.-H. Deng, M. L. Klein, and G. J. Martyna, J. Chem. Soc. Faraday Trans. **90**, 2009 (1994); Z.-H. Deng, G. J. Martyna, and M. L. Klein, J. Chem. Phys. **100**, 7590 (1994); Phys. Rev. Lett. **71**, 267 (1993).
[7] L. M. Falicov and J. C. Kimball, Phys. Rev. Lett. **22**, 997 (1969).
[8] C. J. Thompson, T. Matsubara, and Y. S. Yang, Prog. Theor. Phys. **91**, 251 (1994).
[9] K. A. Dawson, M. D. Lipkin, and B. Widom, J. Chem. Phys. **88**, 5149 (1988); B. Widom, J. Chem. Phys. **90**, 2437 (1989); **84**, 6943 (1986).
[10] G. Gompper and M. Schick, *Self-Assembling Amphiphilic Systems* (Academic Press, San Diego, 1994); M. Kahlweit *et al.*, J. Colloid Interface Sci. **118**, 436 (1987).
[11] U. Brandt and C. Mielsch, Z. Phys. B **75**, 365 (1989); **79**, 295 (1990); **82**, 37 (1991).
[12] J. W. Negele and H. Orland, *Quantum Many-Particle Systems* (Addison-Wesley, Redwood City, 1988).
[13] D. Belitz and T. R. Kirkpatrick, Rev. Mod. Phys. **66**, 261 (1994).
[14] $\rho_b = \{1 + \exp[-\mu_b + \bar{\sigma} + 2\ln(1 + e^{-\mu_e(1-\alpha)}) - w_o\rho_b]\}^{-1}$ is an explicit function of μ_e, and $\bar{f}$ must also be optimized with respect to α to obtain $\rho_e = (1 - \rho_b)\bar{\rho}_e$.
[15] S. E. Barnes, J. Phys. F **7**, 2637 (1977); **6**, 1375 (1976).
[16] G. Kotliar and A. E. Ruckenstein, Phys. Rev. Lett. **57**, 1362 (1986).
[17] K. Leung and F. S. Csajka (unpublished).
[18] H.-J. Woo, C. Carraro, and D. Chandler, Phys. Rev. E **52**, 6497 (1995).
[19] J. K. Freericks, Phys. Rev. B **47**, 9263 (1993).
[20] D. N. Knapp and H. D. Bale, J. Appl. Cryst. **11**, 606 (1978).
[21] P. Chieux and H. Bertagnolli, J. Phys. Chem. **88**, 3726 (1984).
[22] In typical microemulsions, $M_2 < 0$; see M. Teubner and R. Strey, J. Chem. Phys. **87**, 3195 (1987).
[23] J. Jortner and M. H. Cohen, J. Chem. Phys. **58**, 5170 (1973).